Eclética Química
ISSN: 0100-4670
ISSN: 1678-4618
ecletica@journal.iq.unesp.br
Universidade Estadual Paulista Júlio de Mesquita Filho
Brasil

Pinatti, Ivo Mateus; de Foggi, Camila Cristina; Teodoro, Marcio Daldin; Longo, Elson; Simões, Alexandre Zirpoli; Rosa, Ieda Lúcia Viana
YVO4:RE (RE = Eu, Tm, and Yb/Er) nanoparticles synthesized by the microwave-assisted hydrothermal method for photoluminescence application
Eclética Química, vol. Esp. 47, núm. 1, 2022, pp. 39-49
Universidade Estadual Paulista Júlio de Mesquita Filho
Araraquara, Brasil

DOI: https://doi.org/10.26850/1678-4618eqj.v47.1SI.2022.p39-49

Disponible en: https://www.redalyc.org/articulo.oa?id=42973868005

Eclética Química Journal

Original article

revista.iq.unesp.br

| Vol. 47 | special issue 1 | 2022 |

YVO_4:RE (RE = Eu, Tm, and Yb/Er) nanoparticles synthesized by the microwave-assisted hydrothermal method for photoluminescence application

Ivo Mateus Pinatti[1+], Camila Cristina de Foggi[2], Marcio Daldin Teodoro[3], Elson Longo[4], Alexandre Zirpoli Simões[1], Ieda Lúcia Viana Rosa[4]

1. São Paulo State University, Faculty of Engineering, Guaratinguetá, Brazil.
2. Federal University of Rio Grande do Sul, School of Dentistry, Porto Alegre, Brazil.
3. Federal University of São Carlos, Department of Physics, São Carlos, Brazil.
4. Federal University of São Carlos, Center for the Development of Functional Materials, São Carlos, Brazil.

+Corresponding author: Ivo Mateus Pinatti, **Phone:** +55 16 33518214, **Email address:** ivopinatti@hotmail.com

ARTICLE INFO

Article history:
Received: July 29, 2021
Accepted: October 11, 2021
Published: April 11, 2022

Section Editors: Elson Longo and Juan Manuel Andrés Bort

Keywords:
1. yttrium vanadate
2. rare earth
3. photoluminescence
4. semiconductor

ABSTRACT: Here, an experimental study is presented on the YVO4:RE (RE = Eu, Tm, and Yb/Er) nanoparticles synthesized by means of the microwave-assisted hydrothermal method. Different characterization techniques (X-ray diffraction, Raman and ultraviolet-visible spectroscopy, field emission scanning electron microscopy, transmission electron microscopy, and photoluminescence emissions) have been employed to examine the structural, optical, as well as its morphology and photoluminescent properties. The as-synthetized samples present different emission colors due to RE^{3+} ions, as well as nanosized spherical morphology because of synthesis method. These materials can be considered efficient materials for optical devices.

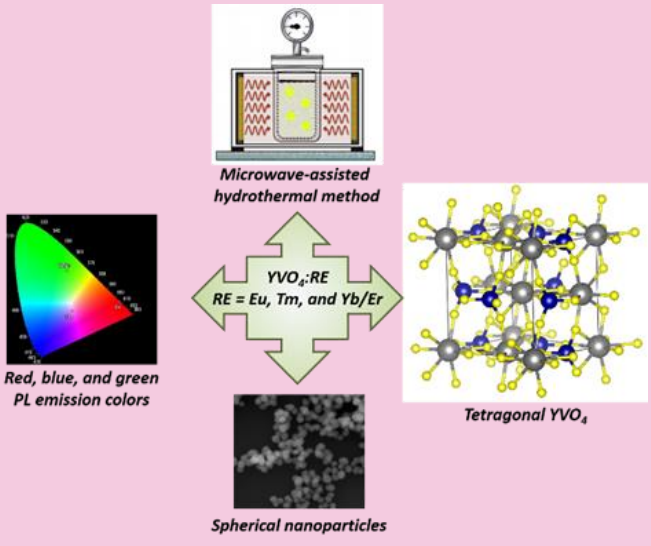

ISSN: 1678-4618
DOI: 10.26850/1678-4618eqj.v47.1SI.2022.p39-49

1. Introduction

Photoluminescent (PL) materials with high quantum efficiency present practical applications in many research areas, such as optoelectronics, medicine, biolabels, physics, among others (Ferreira *et al.*, 2018; Panayiotakis *et al.*, 1996; Shen *et al.*, 2010). Consequently, several inorganic matrices are studied, in which its PL property was deeply explored due to its host lattice composition, structure, morphology as well as doping and others crystal modifications (Li *et al.*, 2021). Ideally, these materials may present well-defined characteristics such as size, optical properties, and a wide range of emission colors (Liu *et al.*, 2016).

Moreover, visible-emitting phosphors can be achieved by doping different kinds of rare earth (RE) ions into lanthanide orthovanadates. The orthovanadate matrix absorbs in the ultraviolet region of electromagnetic spectrum due to ligand-metal charge transfer (LMCT) from the 2p orbital in O^{2-} to the 3d orbital in vanadate. The YVO_4 nanoparticles, as an example, are an ideal transparent host lattice for PL activators and present low toxicity in biological medium (Rivera-Enríquez and Fernández-Osorio, 2021). YVO_4 also presents relative low phonon energy, excellent thermal, mechanical, and chemical stability and high optical performance. Furthermore, the D_{2d} local point symmetry of the eight-coordinated Y^{3+} ion in the tetragonal crystal structure (space group D_{4h}) is an ideal doping site for RE^{3+} ions (Liu *et al.*, 2015). For instance, controlled fabrication of YVO_4:Eu^{3+} nanoparticles and nanowires were achieved by microwave assisted chemical synthesis (Huong *et al.*, 2016).

Several works related the doping of RE^{3+} ions into different types of inorganic matrices (Pinatti *et al.*, 2015; 2016; 2019a; 2019b; Yang *et al.*, 2018). The RE emissions arise from the 4f–4f or 5d–4f transitions from the UV to near-IR range of electromagnetic spectrum. Also, upconverting (UC) materials are an unprecedented technology which consists of absorption of two or more lower-energy photons and subsequently emission of one higher-energy photon. This strategy is specially used for solar energy materials, bioimaging, among other applications. Materials composed of Yb^{3+}/Er^{3+} as activator ions can be efficiently excited using NIR (near-infrared) laser radiation to generate visible emission. For example, photostable and small YVO_4:Yb/Er upconversion nanoparticles in water were obtained and presented intense upconversion emission (Alkahtani *et al.*, 2021). However, many of these materials present poor luminescence efficiency and/or complicated synthesis procedure, which results in no defined or irregular sizes particles (Ji *et al.*, 2021; Kshetri *et al.*, 2018; Sousa Filho *et al.*, 2019; Woźny *et al.*, 2019).

Accordingly, in this work, we report the synthesis of YVO_4:RE (RE = Eu, Tm, and Yb/Er) nanoparticles by the microwave-assisted hydrothermal (MAH) method. These nanoparticles were structurally characterized and potentially studied in terms of its PL properties. In addition, the structure, vibrational frequency and morphology are compared to rationalize the structure, morphology, and PL emissions.

2. Experimental

2.1 Synthesis

One mmol of NH_4VO_3 (99%, Sigma-Aldrich) was dissolved in 40 mL of distilled water at room temperature under magnetic stirring until the reagent was completely dissolved. Additionally, 2 mmol of $Y(NO_3)_3{\cdot}4H_2O$ (99.999%, Sigma-Aldrich) was dissolved in 40 mL of distilled water at room temperature. $RE(NO_3)_3$ (RE = Eu, Tm, Yb, and Er) solutions were prepared by dissolving RE_2O_3 in aqueous hot solution of HNO_3 and evaporating the excess of acid. Stoichiometric volume of RE solutions were mixed together with the Y solution. The amount of 5 mol% of Eu^{3+}, and Tm^{3+}; and 5 mol%Yb^{3+}/2 mol%Er^{3+} were chosen due to previous works related to maximum PL emission intensity achieved. After complete dissolution of the reactants, the V solution was mixed with the Y solution to obtain YVO_4 and with the Y/RE solution to obtain YVO_4:RE nanoparticles. Subsequently, the mixture was stirred for 10 min, and, thereafter, it was transferred to the MAH system at 160 °C for 32 min, as it was the ideal conditions for many materials obtained by this methodology. The precipitates formed were collected at room temperature, washed with distilled water until the pH was neutralized, and dried in a conventional furnace at 60 °C for 12 h. Figure 1 shows a representation of the synthesis procedure herein described.

ISSN: 1678-4618
DOI: 10.26850/1678-4618eqj.v47.1SI.2022.p39-49

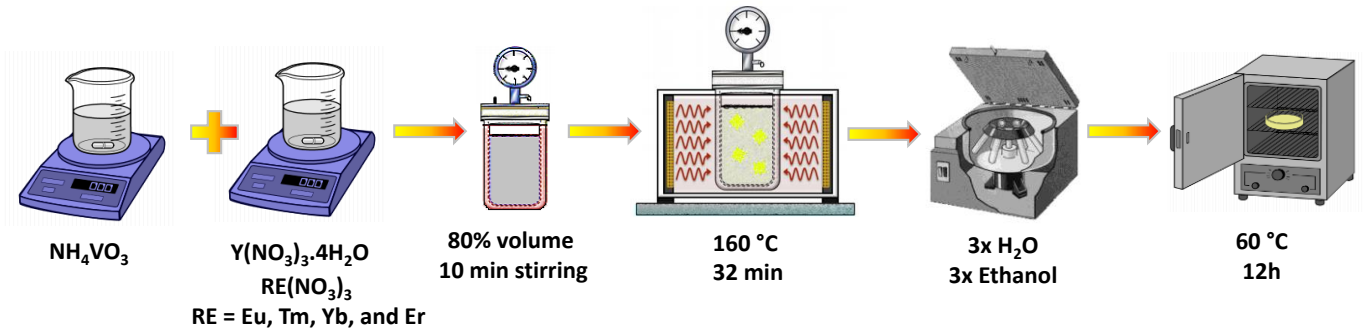

Figure 1. Schematic representation of synthesis procedure of the nanoparticles.

2.2 Characterizations

The nanoparticles were structurally characterized by X-ray diffraction (XRD) patterns using a D/Max-2000PC diffractometer Rigaku (Japan) with Cu Kα radiation (λ = 1.5406 Å) in the 2θ range from 10° to 80° in the normal routine, with a scanning velocity of 2° min^{-1}. This unit cell was modelled using the visualization for electronic and structural analysis (VESTA) program (Momma and Izumi, 2008; 2011), version 3. Micro-Raman spectroscopy was conducted on a Horiba Jobin-Yvon (Japan) spectrometer charge-coupled device detector and argon-ion laser (Melles Griot, United States) operating at 532 nm with a maximum power of 200 mW. The ultraviolet-visible spectrophotometry (UV-vis) spectra were taken using a spectrophotometer (model Cary 5G) (Varian, USA) in diffuse-reflectance mode. Morphological analysis of the particles was recorded via field-emission scanning electron microscopy (FE-SEM) using a Carl Zeiss microscope (model Supra 35) operated at an accelerating voltage of 30 kV and a working distance of 3.7 mm. Transmission electron microscopy (TEM) and high-resolution transmission electron microscopy (HRTEM) analysis was performed using a Jeol JEM-2100F with a field-emission gun (FEG) operating at 200 kV. For the micrographs, the samples (approximately 1 mg) were dispersed in 3 mL of distilled water and kept 15 min in the ultrasound bath. Then, one drop of the suspension was deposited on a silicon wafer, dried at room temperature and finally attached to a sample stub using carbon tape for FE-SEM analysis; and one drop of the suspension was deposited on the cupper grid and dried at room temperature for TEM analysis. Photoluminescence (PL) measurements were performed by two distinct equipment. In the first one, the samples were excited by a 355 nm laser (Cobolt/Zouk) focused on a 20 μm spot, 50 μW of power. The backscattered luminescence was dispersed by a 20 cm spectrometer with the signal detected by a charged coupled device detector (Andor technologies). In the second one, the PL spectra were carried out with 325 nm excitation source of a krypton ion laser (Coherent Innova) and 200 mW laser output, at monochromator Thermal Jarrel-Ash Monospec and a Hamamatsu R446 photomultiplier. All measurements were performed at room temperature.

3. Results and discussion

3.1 X-ray diffraction patterns

Figure 2 shows the XRD patterns of YVO_4:RE, and all the diffraction peaks can be readily indexed to the pure tetragonal YVO_4 phase (PDF No. 17-0341) (Rivera-Enríquez and Fernández-Osorio, 2021; Yu *et al.*, 2002). The intense and sharp peaks confirm the samples are pure and present high crystallinity, as well as structural long-range order. Also, Y^{3+} site is an ideal environment with a D_{2d} point symmetry for RE emitter. So, effectively Y-by-RE substitution occurs in the host lattice because RE^{3+} and Y^{3+} have similar ionic radius, as widely reported by many works (Matos *et al.*, 2016; Rivera-Enríquez and Fernández-Osorio, 2021). This substitution was not perceived on the XRD patterns due to the limitation of detection of the XRD instrument.

A representation of the unit cell for the orthorhombic YVO_4:RE nanoparticles are presented in Fig. 3. This unit cell was modelled using the lattice parameters and atomic positions, as well as the possible RE-by-Y substitution. The Y/RE coordination environment is a distorted dodecahedral $[YO_8]/[REO_8]$ clusters, while V is a distorted tetrahedral $[VO_4]$ cluster.

ISSN: 1678-4618
DOI: 10.26850/1678-4618eqj.v47.1SI.2022.p39-49

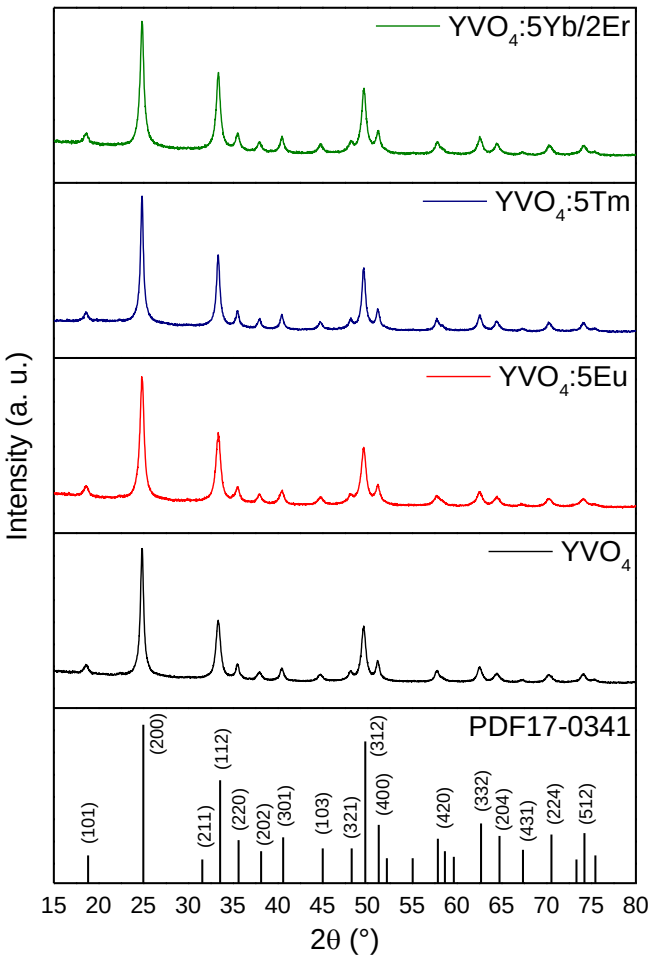

Figure 2. X-ray diffraction patterns of the YVO_4:RE nanoparticles.

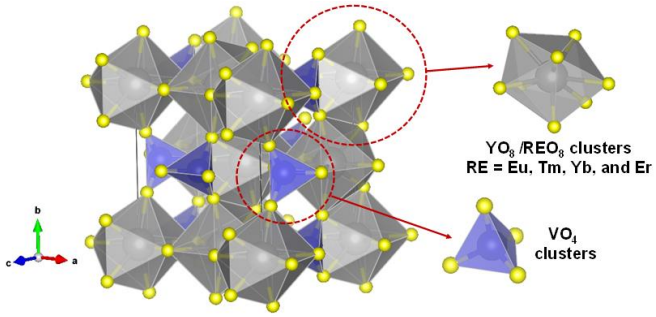

Figure 3. Unit cell representation of YVO_4:RE nanoparticles. Gray, blue, and yellow balls are Y/RE, V and O atoms, respectively.

3.2 Raman spectroscopy

Figure 4 shows the room temperature Raman spectra of YVO_4:RE nanoparticles excited by a green laser. Experimentally, seven active Raman modes were observed at 155, 260, 367, 482, 796, 820, and 874 cm^{-1} for the YVO_4, YVO_4:5Eu, and YVO_4:5Tm samples. For the YVO_4:5Yb/2Er, six active Raman modes were observed at 328, 402, 638, 796, 818, and 871 cm^{-1}. Also, the YVO_4:5Yb/2Er nanoparticle present a broad PL emission, as observed in the Raman spectra, due to the Yb/Er ions. These results confirm the structural short-range order of all samples (Jayaraman *et al.*, 1987).

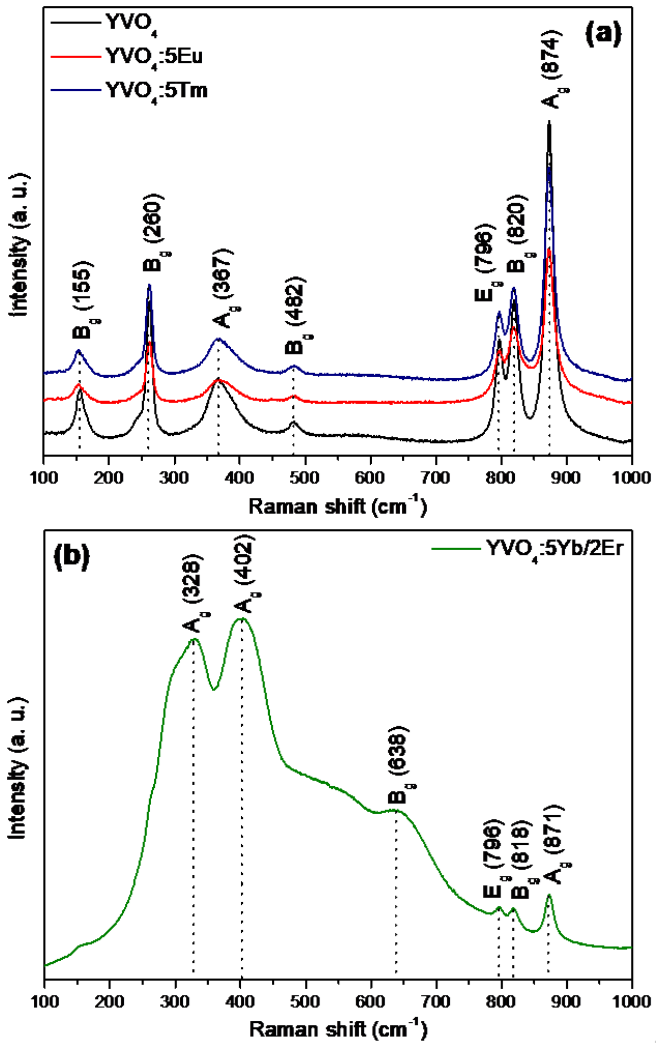

Figure 4. Raman spectra of the **(a)** YVO_4:RE (RE = Eu and Tm), and **(b)** YVO_4:5Yb/2Er nanoparticles.

3.3 UV-vis spectroscopy

Figure 5 illustrates the UV-vis diffuse reflectance spectra of the YVO_4:RE nanoparticles in the range of 275–750 nm. The samples showed absorption in the ultraviolet region at approximately 450 nm. The absorption is a result of electronic transition between the valence band (VB) formed predominantly by O 2p state, and the conduction band (CB) composed mainly by V 3d states (Yang *et al.*, 2018). Also, the YVO_4:5Tm sample present the $^3H_6 \rightarrow {}^3F_3$ transition, and the YVO_4:5Yb/2Er present the $^4I_{15/2} \rightarrow {}^2H_J$ (J = 11/2 and 9/2) transitions.

Eclética Química Journal, vol. 47, special issue 1, 2022, 39-49
ISSN: 1678-4618
DOI: 10.26850/1678-4618eqj.v47.1SI.2022.p39-49

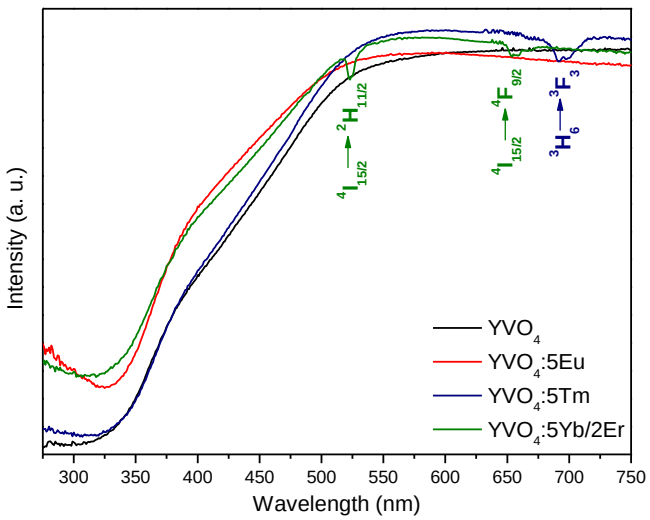

Figure 5. The UV-vis diffuse reflectance spectra of the YVO_4:RE nanoparticles.

The band gap energy (E_{gap}) values were calculated using the relation of the Kubelka–Munk and Wood Tauc function, as previously reported (Pinatti *et al.*, 2019a), and it was obtained by linear extrapolation of the UV-vis curve in the $[F(R_\infty)hv]^n$ versus hv graph. $F(R_\infty)$ is the Kubelka–Munk function, hv is the photon energy, and n is a constant related to the type of electronic transition of a semiconductor (n = 0.5 for direct allowed, n = 2 for indirect allowed, n = 1.5 for direct forbidden, and n = 3 for indirect forbidden). The theoretical calculation predicts a direct allowed transition for YVO_4. Thus, the E_{gap} values obtained were 3.54, 3.41, 3.46, and 3.39 eV for the YVO_4, YVO_4:5Eu, YVO_4:5Tm, and YVO_4:5Yb/2Er samples, respectively (Fig. 6). These results show that the E_{gap} values decrease due to insertion of the RE ions, indicating that the degree of order-disorder at electronic level were affected due to Y-by-RE substitution. This behavior was previously observed in other RE doped materials and is attributed mainly by the contribution of $4f^n$ electrons of RE^{3+} ions either to the VB or CB, which can increase the covalent bonding of V−O and reduce the E_{gap}. This happens because the energy level of RE^{3+} ions matches the energy level of VO_4^{3-}, contributing to an effective energy transfer from the VO_4^{3-} to the excited states of RE^{3+} ions (Yang *et al.*, 2018).

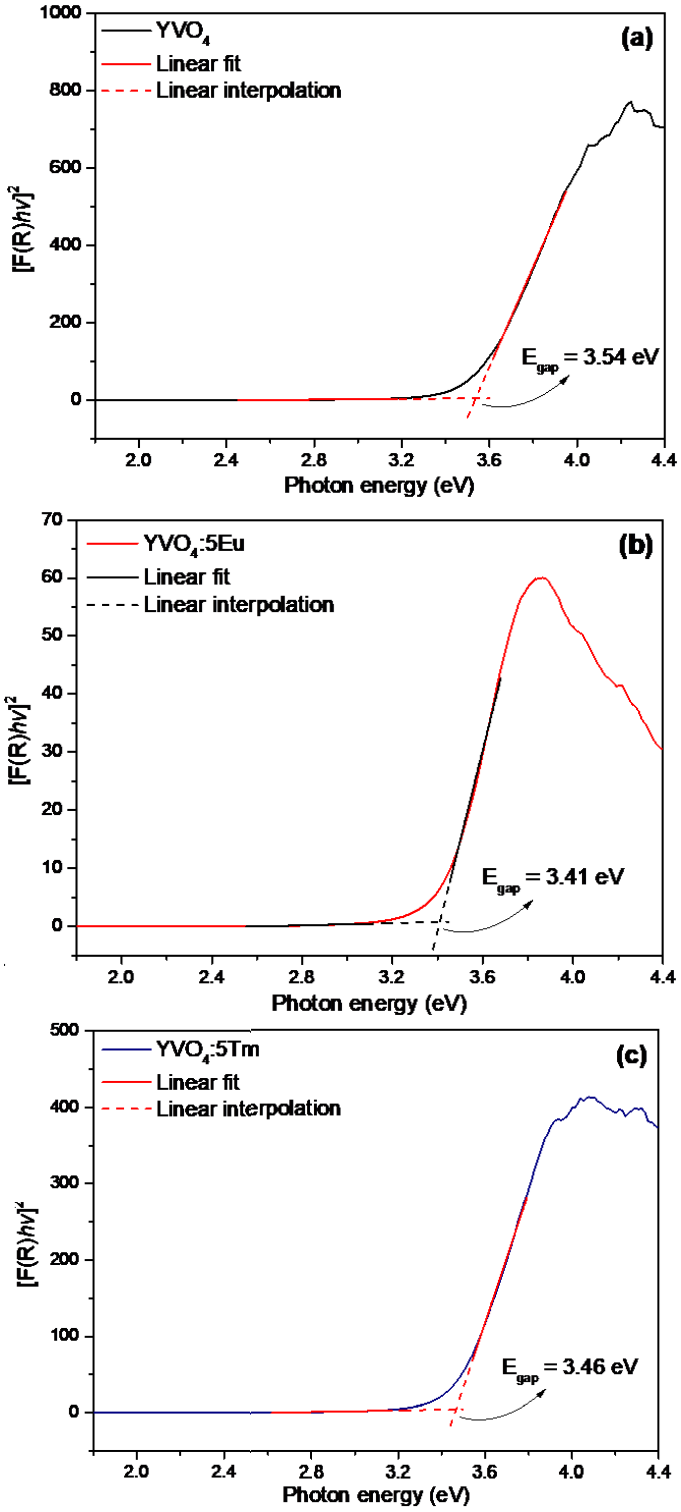

Eclética Química Journal, vol. 47, special issue 1, 2022, 39-49
ISSN: 1678-4618
DOI: 10.26850/1678-4618eqj.v47.1SI.2022.p39-49

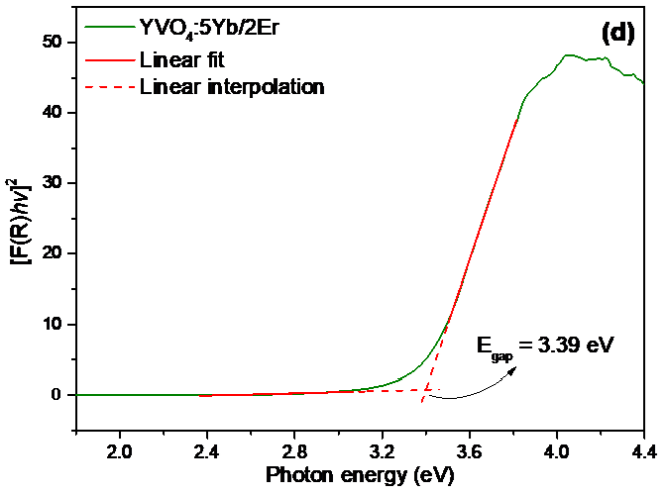

Figure 6. Band gap energy (E_{gap}) for the YVO_4:RE nanoparticles.

3.4 Field-emission scanning electron microscopy and TEM

The detailed morphology and particle size of YVO_4 nanoparticles were assessed by FE-SEM, and the nanostructures were further characterized by TEM and HRTEM. Field emission scanning electron microscopy micrographs of the YVO_4 nanoparticles are shown in Fig. 7a and b. It is clearly seen spherical nanoparticles which exhibit a high degree of homogeneity in the shape and size. As shown in Fig. 7a and b, the particles present smooth surface, well-defined shape, and are mainly aggregated with a monodisperse size distribution.

Figure 7c shows the TEM image of YVO_4 nanoparticles. It was mainly observed spherical-like particles of sizes ranging from 20 to 50 nm. Most of them have perfect circular morphology, while other present small deformations. Figure 7d shows the HRTEM image of YVO_4 nanoparticles. The YVO_4 nanoparticles presented a single crystalline nature and the lattice spacing was calculated to be 0.363 nm between two adjacent lattice fringes, which could be indexed to 200 planes of zircon-type YVO_4. This is in agreement with the XRD results (Shen *et al.*, 2010). Moreover, the other YVO_4:RE samples also showed similar morphology and as single-crystalline and this can be attributed to the similar preparative conditions and the low dopant concentration of RE^{3+} ions (data not shown).

These results confirm that nanosized YVO_4 of spherical morphology can be obtained by the MAH method at short reactional time and low temperature. Moreover, this morphology, as well as the size, are effectively acquired without the use of surfactants, templates, organic solvents, or adjustment of pH value of the medium, which is usually required to obtain homogeneous and nanosized particles.

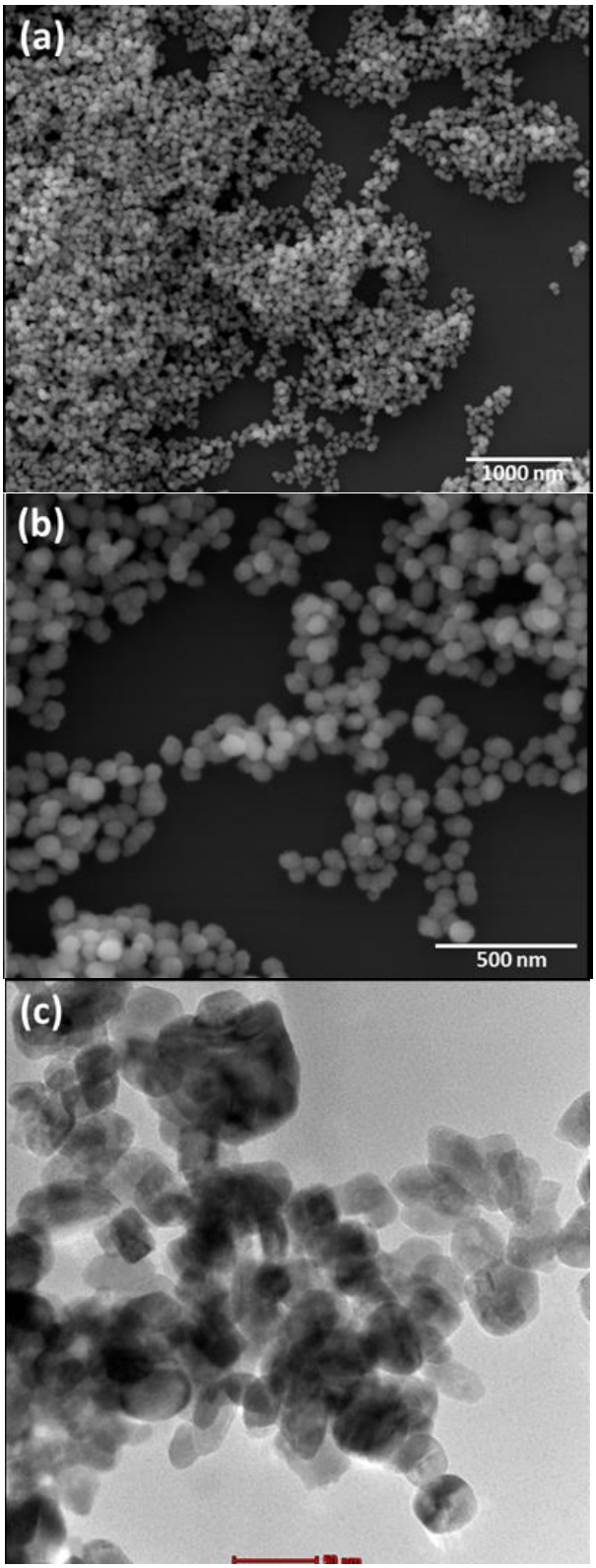

Eclética Química Journal, vol. 47, special issue 1, 2022, 39-49
ISSN: 1678-4618
DOI: 10.26850/1678-4618eqj.v47.1SI.2022.p39-49

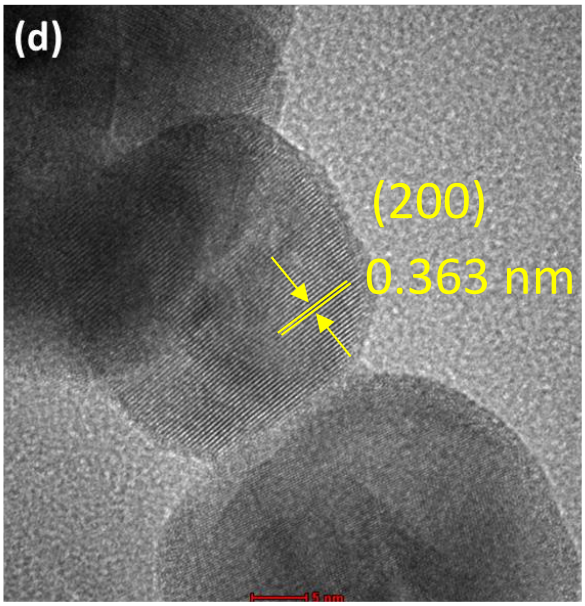

Figure 7. (a, b) FE-SEM images, **(c)** TEM image, and **(d)** HRTEM image of YVO_4 nanoparticles.

3.5 Photoluminescence spectroscopy

Figure 8 shows the PL emission spectra at room temperature of YVO_4:RE nanoparticles under the excitation wavelength of 355 nm. Figure 8a shows the PL emission spectra of YVO_4:RE (RE = Tm, and Yb/Er) nanoparticles, presenting an intense band at 540 nm due to VO_4^{3-} clusters (Jin *et al.*, 2011), and the YVO_4:5Tm nanoparticles also present the $^3H_4 \rightarrow {}^3H_6$ transition at 806 nm. Particularly, the YVO_4:Eu nanoparticles present intense $^5D_1 \rightarrow {}^7F_J$ (J = 1 and 2) and $^5D_0 \rightarrow {}^7F_J$ (J = 1–4) transitions, which arises due to the efficient energy transfer from VO_4^{3-} clusters to the Eu^{3+} ions (see Fig. 8b) (Matos *et al.*, 2016; Pinatti *et al.*, 2019a; Saltarelli *et al.*, 2014).

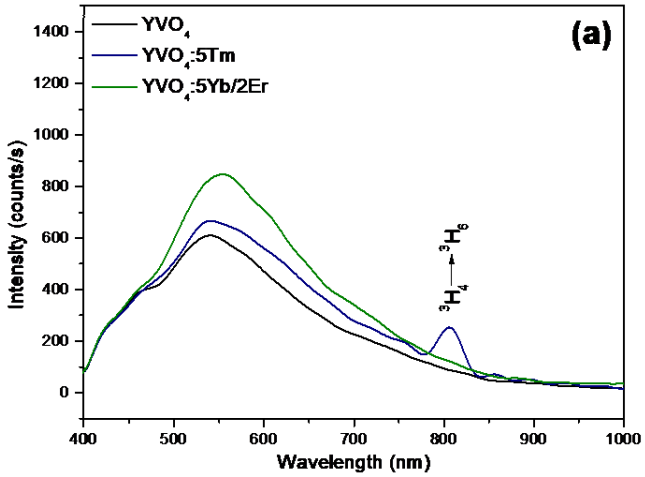

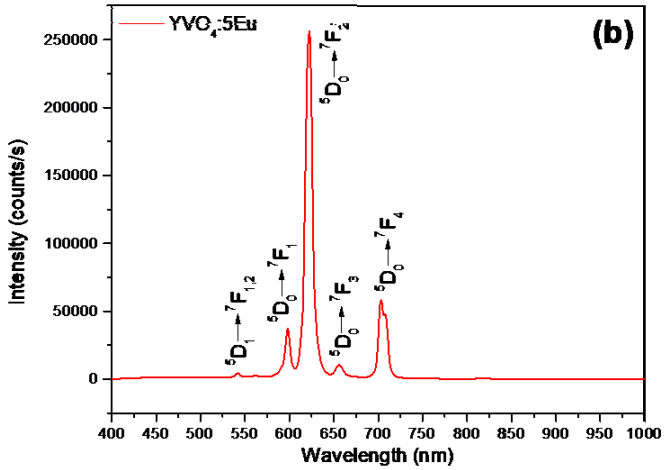

Figure 8. Photoluminescent emission spectra of **(a)** YVO_4:RE (RE = Tm and Yb/Er), and **(b)** YVO_4:5Eu nanoparticles.

Figure 9 shows the PL emission spectra at room temperature of YVO_4:RE nanoparticles under the excitation wavelength of 325 nm, as well as the CIE chromatic diagram. Figure 9a shows the PL emission spectra of the YVO_4:5Eu nanoparticles, which presents characteristic Eu^{3+} peaks at 543, 564, 595, 622, 655, and 705 nm ascribed to the $^5D_1 \rightarrow {}^7F_J$ (J = 1 and 2), and $^5D_0 \rightarrow {}^7F_J$ (J = 1–4) transitions, respectively (Almeida *et al.*, 2021; Pinatti *et al.*, 2015). Figure 9b shows the PL emission spectra of the YVO_4:5Tm nanoparticles, which present characteristic Tm^{3+} peaks at 480, 548, 650, and 795 nm related to the $^1D_2 \rightarrow {}^3F_J$ (J = 4 and 5), $^1G_4 \rightarrow {}^3F_4$, and $^3H_4 \rightarrow {}^3H_6$ transitions, respectively (Pinatti *et al.*, 2019a). Figure 9c shows the PL emission spectra of the YVO_4:5Yb/2Er nanoparticles, which present characteristic Er^{3+} peaks at 530, 555, and 671 nm attributed to the $^2H_{11/2} \rightarrow {}^4I_{15/2}$, $^4S_{3/2} \rightarrow {}^4I_{15/2}$, and $^4F_{9/2} \rightarrow {}^4I_{15/2}$ transitions, respectively (Alkahtani *et al.*, 2021; Mahata *et al.*, 2015; Sun *et al.*, 2006; Woźny *et al.*, 2018; Zhang *et al.*, 2010). Figure 9d shows the CIE chromatic diagram and the respective positions of x, and y coordinates of the YVO_4:RE (RE = Eu, Tm, and Yb/Er) nanoparticles obtained through the PL emission spectra. The (x;y) chromatic coordinates positions are listed in Tab. 1. The YVO_4:5Eu, YVO_4:5Tm, and YVO_4:5Yb/2Er nanoparticles present intense emitting color in the red, blue, and green region of the diagram, respectively. These results confirm the pureness and brightness of the samples and can be considered as optimum materials for optical devices.

Eclética Química Journal, vol. 47, special issue 1, 2022, 39-49
ISSN: 1678-4618
DOI: 10.26850/1678-4618eqj.v47.1SI.2022.p39-49

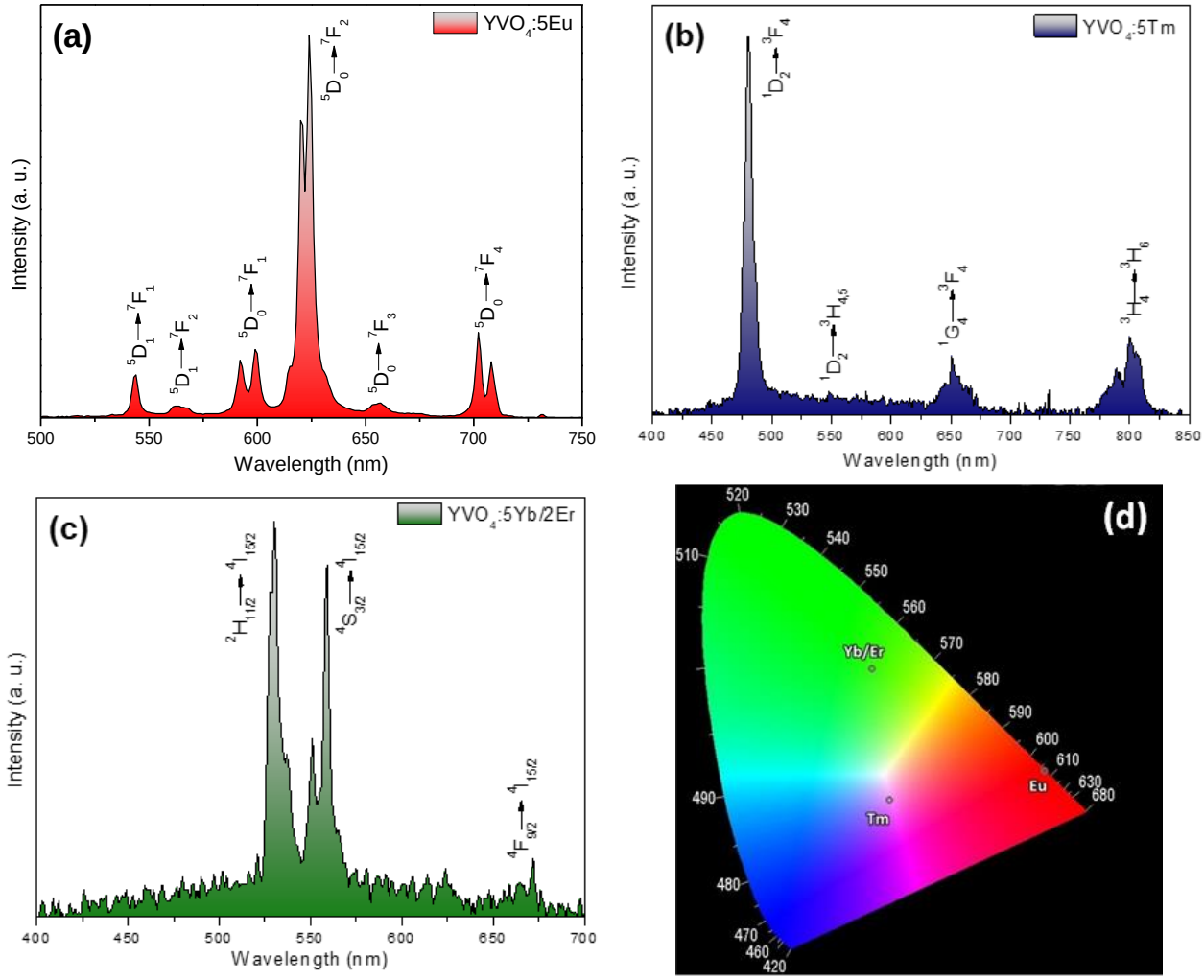

Figure 9. Photoluminescent emission spectra of **(a)** YVO_4:5Eu, **(b)** YVO_4:5Tm, **(c)** YVO_4:5Yb/2Er nanoparticles, and **(d)** CIE chromatic diagram.

Table 1. Chromatic coordinates values obtained by the PL emission spectra of the YVO_4:RE nanoparticles.

Samples	Chromatic coordinates	
	x	y
YVO_4:5Eu	0.65	0.34
YVO_4:5Tm	0.36	0.29
YVO_4:5Yb/2Er	0.33	0.53

Figure 10 shows a schematic energy level diagram and a proposed energy transfer mechanism for the YVO_4:RE nanoparticles. For the YVO_4:5Eu nanoparticles, it is observed that, under excitation at 325 nm, electrons are excited from VB into the charge transfer state (CTS) of the VO_4^{3-} clusters. Then, the excitation energy is transferred from the VO_4^{3-} group to the $^5D_4$ level of Eu^{3+} cations. Afterwards, Eu^{3+} cations in the populated $^5D_4$ level undergo multiphonon relaxation to the $^5D_1$ level that radiatively decay to the ^7F_J (J = 1 and 2) levels; and to the $^5D_0$ level that radiatively decay to the ^7F_J (J = 1–4) levels. For the YVO_4:5Tm nanoparticles, the excitation energy is transferred from the VO_4^{3-} group to the $^3P_2$ level of Tm^{3+} cations. Then, Tm^{3+} cations in the populated $^3P_2$ level undergo multiphonon relaxation to the $^1D_2$ level that radiatively decay to the $^7F_4$ and $^3H_4$ levels; and to the $^1G_4$ level that radiatively decay to the $^7F_4$ and $^3H_6$ levels. Finally, for the YVO_4:5Yb/2Er nanoparticles, the excitation energy is transferred from the VO_4^{3-} group to the $^4F_{7/2}$ level of Er^{3+} cations. Then, Er^{3+} cations in the populated $^4F_{7/2}$ level undergo multiphonon relaxation to the $^2H_{11/2}$ and $^4S_{3/2}$ levels that radiatively decay to the $^4I_{15/2}$ level; and to the $^4F_{9/2}$ level that radiatively decay to the $^4I_{15/2}$ level. Alternatively, according to the energy conservation law, a two-photon process can occur and populate the green and red UC emissions of Er^{3+} ions. The successive energy transfers are: $^4I_{15/2}$ (Er^{3+}) + $^2F_{5/2}$ (Yb^{3+}) → $^4I_{11/2}$ (Er^{3+}) + $^2F_{7/2}$ (Yb^{3+}) and $^4I_{11/2}$ (Er^{3+}) + $^2F_{5/2}$ (Yb^{3+}) → $^4F_{7/2}$ (Er^{3+}) + $^2F_{7/2}$ (Yb^{3+}) excite Er^{3+} ions to the $^4F_{7/2}$ state. Er^{3+}

Eclética Química Journal, vol. 47, special issue 1, 2022, 39-49
ISSN: 1678-4618
DOI: 10.26850/1678-4618eqj.v47.1SI.2022.p39-49

ions at the $^2H_{11/2}/^4S_{3/2}$ states, arising from the nonradiative relaxation (NR) process of the $^4F_{7/2}$ state, radiatively decay to the $^4I_{15/2}$ state, resulting the green UC emissions. The $^4F_{9/2}$ red emitting state is populated by the process: $^4I_{13/2}$ (Er^{3+}) + $^2F_{5/2}$ (Yb^{3+}) → $^4F_{9/2}$ (Er^{3+}) + $^2F_{7/2}$ (Yb^{3+}), where the $^4I_{13/2}$ state is populated by NR process of the $^4I_{11/2}$ state (Ji *et al*., 2021).

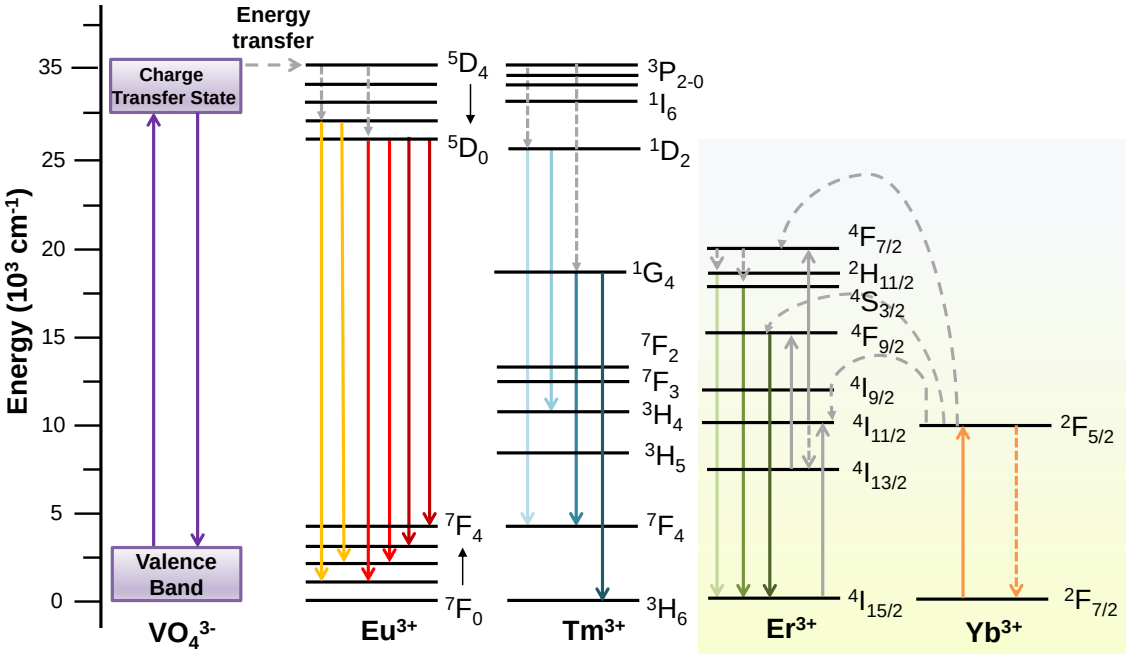

Figure 10. Schematic energy level diagram and a proposed energy transfer mechanism for the YVO_4:RE nanoparticles. Solid arrows = radiative transition, dashed arrows = energy transfer, and dotted arrows = nonradiative transition.

4. Conclusions

In summary, we reported the efficient synthesis of YVO_4:RE nanoparticles by the microwave-assisted hydrothermal method. Long-range order was confirmed by XRD patterns, which showed sharp and well-defined peaks with no segregated materials. Vibrational Raman modes observed represent a signature of the structural organization in the short-range. The UV-vis spectra indicate that the band gap value decreases due to RE doping attesting structural order-disorder of the materials. The FE-SEM, TEM, and HRTEM images prove that the materials are spherical and in the nanoscale size. Photoluminescent emission spectra present transitions in the red, blue, and green regions, attesting these materials as good phosphors in the visible region. Also, the YVO_4:5Yb/2Er is a good candidate as promising material for UC phosphor.

Authors' contribution

Conceptualization: Pinatti, I. M.; Foggi, C. C.; Teodoro, M. D.; Longo, E.; Simões, A. Z.; Rosa, I. L. V.
Data curation: Pinatti, I. M.; Foggi, C. C.; Teodoro, M. D.; Longo, E.; Simões, A. Z.; Rosa, I. L. V.
Formal Analysis: Pinatti, I. M.; Foggi, C. C.; Teodoro, M. D.; Longo, E.; Simões, A. Z.; Rosa, I. L. V.
Funding acquisition: Pinatti, I. M.; Foggi, C. C.; Teodoro, M. D.; Longo, E.; Simões, A. Z.; Rosa, I. L. V.
Investigation: Pinatti, I. M.; Foggi, C. C.; Teodoro, M. D.; Longo, E.; Simões, A. Z.; Rosa, I. L. V.
Methodology: Pinatti, I. M.; Foggi, C. C.; Teodoro, M. D.; Longo, E.; Simões, A. Z.; Rosa, I. L. V.
Project administration: Pinatti, I. M.; Foggi, C. C.; Teodoro, M. D.; Longo, E.; Simões, A. Z.; Rosa, I. L. V.
Resources: Pinatti, I. M.; Foggi, C. C.; Teodoro, M. D.; Longo, E.; Simões, A. Z.; Rosa, I. L. V.
Software: Not applicable.
Supervision: Longo, E.; Simões, A. Z.; Rosa, I. L. V.
Validation: Pinatti, I. M.; Foggi, C. C.; Teodoro, M. D.; Longo, E.; Simões, A. Z.; Rosa, I. L. V.
Visualization: Pinatti, I. M.; Foggi, C. C.; Teodoro, M. D.; Longo, E.; Simões, A. Z.; Rosa, I. L. V.

Eclética Química Journal, vol. 47, special issue 1, 2022, 39-49
ISSN: 1678-4618
DOI: 10.26850/1678-4618eqj.v47.1SI.2022.p39-49

Writing – original draft: Pinatti, I. M.; Foggi, C. C.; Teodoro, M. D.; Longo, E.; Simões, A. Z.; Rosa, I. L. V.
Writing – review & editing: Pinatti, I. M.; Foggi, C. C.; Teodoro, M. D.; Longo, E.; Simões, A. Z.; Rosa, I. L. V.

Data availability statement

The data will be available upon request.

Funding

Fundação de Amparo à Pesquisa do Estado de São Paulo (FAPESP). Grant No.: 13/07296-2; 17/12594-3; 19/03722-3; 19/25944-8.

Acknowledgments

The authors would like to acknowledge Maximo Siu Li (IFSC-USP), Rorivaldo Camargo (CDMF-UFSCar), and Sandra Maria Terenzi Bellini (CDMF-UFSCar) for technical and scientific contributions.
This manuscript is dedicated to the memory of Professor Dr. José Arana Varela, pioneer with notable achievements in the fields of materials science, physics and chemistry. He was one of the founders of the Interdisciplinary Laboratory of Electrochemistry and Ceramics (LIEC), Brazil. Dr. Varela contributed significantly to the development of Brazilian science, and had an outstanding international reputation as an educator and researcher.

References

Alkahtani, M.; Alfahd, A.; Alsofyani, N.; Almuqhim, A. A.; Qassem, H.; Alshehri, A. A.; Almughen, F. A.; Hemmer, P. Photostable and small YVO_4:Yb,Er upconversion nanoparticles in water. *Nanomaterials* **2021**, *11* (6), 1535. https://doi.org/10.3390/nano11061535

Almeida, P. B.; Pinatti, I. M.; Oliveira, R. C.; Teixeira, M. M.; Santos, C. C.; Machado, T. R.;Longo, E.; Rosa, I. L. V. Structural, morphological and photoluminescence properties of β-Ag_2MoO_4 doped with Eu^{3+}. *Chem. Pap.* **2021**, *75*, 1869–1882. https://doi.org/10.1007/s11696-020-01489-4

Ferreira, N. H.; Furtado, R. A.; Ribeiro, A. B.; Oliveira, P. F.; Ozelin, S. D.; Souza, L. D. R.; Rinaldi Neto, F.; Miura, B. A.; Magalhães, G. M.; Nassar, E. J.; Tavares, D. C. Europium(III)-doped yttrium vanadate nanoparticles reduce the toxicity of cisplatin. *J. Inorg. Biochem.* **2018**, 182,9–17. https://doi.org/10.1016/j.jinorgbio.2018.01.014

Huong, T. T.; Vinh, L. T.; Phuong, H. T.; Khuyen, H. T.; Anh, T. K.; Tu, V. D.; Minh, L. Q. Controlled fabrication of the strong emission YVO_4:Eu^{3+} nanoparticles and nanowires by microwave assisted chemical synthesis. *J. Lumin.* **2016**, *173*, 89–93. https://doi.org/10.1016/j.jlumin.2016.01.003

Jayaraman, A.; Kourouklis, G. A.; Espinosa, G. P.; Cooper, A. S.; Van Uitert, L. G. A high-pressure Raman study of yttrium vanadate (YVO_4) and the pressure-induced transition from the zircon-type to the scheelite-type structure. *J. Phys. Chem. Solids* **1987**, *48* (8), 755–759. https://doi.org/10.1016/0022-3697(87)90072-2

Ji, H.; Tang, J.; Tang, X.; Yang, Z.; Zhang, H.; Qian, Y. Enhanced upconversion emissions of $NaNbO_3$:Er^{3+}/Yb^{3+} nanocrystals via Mg^{2+} ions doping. *Mater. Lett.* **2021**, *302*, 130348. https://doi.org/10.1016/j.matlet.2021.130348

Jin, Y.; Li, C.; Xu, Z.; Cheng, Z.; Wang, W.; Li, G.; Lin, J. Microwave-assisted hydrothermal synthesis and multicolor tuning luminescence of $YP_xV_{1-x}O_4$:Ln^{3+} (Ln = Eu, Dy, Sm) nanoparticles. *Mater. Chem. Phys.* **2011**, *129* (1–2), 418–423. https://doi.org/10.1016/j.matchemphys.2011.04.035

Kshetri, Y. K.; Regmi, C.; Kim, H.-S.; Lee, S. W.; Kim, T. H. Microwave hydrothermal synthesis and upconversion properties of Yb^{3+}/Er^{3+} doped YVO_4 nanoparticles. *Nanotechnology* **2018**, *29* (20), 204004. https://doi.org/10.1088/1361-6528/aab2bf

Li, K.; Chen, T.; Mao, H.; Chen, Y.; Wang, J. Preparation and Upconversion Emission Investigation of the YVO_4:Yb^{3+}:Er^{3+} Nanomaterials and Their Coupling with the Au Nanoparticles. *J. Electron. Mater.* **2021**, *50*,1189–1195. https://doi.org/10.1007/s11664-020-08636-3

Liu, Y.; Xiong, H.; Zhang, N.; Leng, Z.; Li, R.; Gan, S. Microwave synthesis and luminescent properties of YVO_4:Ln^{3+} (Ln = Eu, Dy and Sm) phosphors with different morphologies. *J. Alloys Compd.* **2015**, *653*, 126–134. https://doi.org/10.1016/j.jallcom.2015.09.015

Liu, Y.; Yang, C.; Xiong, H.; Zhang, N.; Leng, Z.; Li, R.;Gan, S. Surfactant assisted synthesis of the YVO_4: Ln^{3+} (Ln = Eu, Dy, Sm) phosphors and shape-dependent luminescence properties. *Colloids Surf. A Physicochem. Eng. Asp.* **2016**, *502*, 139–146. https://doi.org/10.1016/j.colsurfa.2016.05.006

Mahata, M. K.; Kumar, K.; Rai, V. K. Er^{3+}–Yb^{3+} doped vanadate nanocrystals: A highly sensitive thermographic phosphor and its optical nanoheater behavior. *Sens. Actuators B Chem.* **2015**, *209*, 775–780. https://doi.org/10.1016/j.snb.2014.12.039

Matos, M. G; Rocha, L. A.; Nassar, E. J.; Verelst, M. Influence of Bi^{3+} ions on the excitation wavelength of the YVO_4:Eu^{3+} matrix. *Opt. Mater.* **2016**, *62*, 12–18. https://doi.org/10.1016/j.optmat.2016.09.035

Momma, K.; Izumi, F. *VESTA*: a three-dimensional visualization system for electronic and structural analysis. *J. Appl. Cryst.* **2008**, *41*, 653–658. https://doi.org/10.1107/S0021889808012016

Momma, K.; Izumi, F. VESTA 3 for three-dimensional visualization of crystal, volumetric and morphology data. *J. Appl. Cryst.* **2011**, *44*, 1272–1276. https://doi.org/10.1107/S0021889811038970

Panayiotakis, G.; Cavouras, D.; Kandarakis, I.; Nomicos, C. A study of X-ray luminescence and spectral compatibility of europium-activated yttrium-vanadate (YVO_4: Eu) screens for medical imaging applications. *Appl. Phys. A* **1996**, *62*, 483–486. https://doi.org/10.1007/BF01567121

Pinatti, I. M.; Nogueira, I. C.; Pereira, W. S.; Pereira, P. F. S.; Gonçalves, R. F.; Varela, J. A.; Longo, E.; Rosa, I. L. V. Structural and photoluminescence properties of Eu^{3+} doped α-Ag_2WO_4 synthesized by the green coprecipitation methodology. *Dalton Trans.* **2015**, *44* (40),17673–17685. https://doi.org/10.1039/C5DT01997D

Pinatti, I. M.; Mazzo, T. M.; Gonçalves, R. F.; Varela, J. A.; Longo, E.; Rosa, I. L. V. $CaTiO_3$ and $Ca_{1-3x}Sm_xTiO_3$: Photoluminescence and morphology as a result of Hydrothermal Microwave Methodology. *Ceram. Int.* **2016**, *42* (1) (Part B), 1352–1360. https://doi.org/10.1016/j.ceramint.2015.09.074

Pinatti, I. M.; Fern, G. R.; Longo, E.; Ireland, T. G.; Pereira, P. F. S.; Rosa, I. L.V.; Silver, J. Luminescence properties of α-Ag_2WO_4 nanorods co-doped with Li^+ and Eu^{3+} cations and their effects on its structure. *J. Lumin.* **2019a**, *206*, 442–454. https://doi.org/10.1016/j.jlumin.2018.10.104

Pinatti, I. M.; Pereira, P. F. S.; Assis, M.; Longo, E.; Rosa, I. L. V. Rare earth doped silver tungstate for photoluminescent applications. *J. Alloys Compd.* **2019b**, *771*, 433–447. https://doi.org/10.1016/j.jallcom.2018.08.302

Rivera-Enríquez, C. E.; Fernández-Osorio, A. L. Synthesis of YVO_4:Eu^{3+} nanophosphors by the chemical coprecipitation method at room temperature. *J. Lumin.* **2021**, *236*, 118110. https://doi.org/10.1016/j.jlumin.2021.118110

Saltarelli, M.; Matos, M. G.; Faria, E. H.; Ciuffi, K. J.; Rocha, L. A.; Nassar, E. J. Preparation of YVO_4:Eu^{3+} at low temperature by the hydrolytic sol–gel methodology. *J. Sol-Gel Sci. Technol.* **2014**, *73*, 283–292. https://doi.org/10.1007/s10971-014-3525-z

Shen, J.; Sun, L. D.; Zhu, J. D.; Wei, L. H.; Sun, H. F.; Yan, C. H. Biocompatible bright YVO_4:Eu nanoparticles as versatile optical bioprobes. *Adv. Funct. Mater.* **2010**, *20* (21), 3708–3714. https://doi.org/10.1002/adfm.201001264

Sousa Filho, P. C.; Alain, J.; Leménager, G.; Larquet, E.; Fick, J.; Serra, O. A.; Gacoin, T. Colloidal Rare Earth Vanadate Single Crystalline Particles as Ratiometric Luminescent Thermometers. *J. Phys. Chem. C* **2019**, *123* (4), 2441–2450. https://doi.org/10.1021/acs.jpcc.8b12251

Sun, Y.; Liu, H.; Wang, X.; Kong, X.; Zhang, H. Optical spectroscopy and visible upconversion studies of YVO_4:Er^{3+} nanocrystals synthesized by a hydrothermal process. *Chem. Mater.* **2006**, *18*, 2726–2732. https://doi.org/10.1021/cm051971m

Woźny, P.; Szczeszak, A.; Lis, S. Effect of various surfactants on changes in the emission color chromaticity in upconversion YVO_4: Yb^{3+}, Er^{3+} nanoparticles. *Opt. Mater.* **2018**, *76*, 400–406. https://doi.org/10.1016/j.optmat.2018.01.009

Woźny, P.; Runowski, M.; Lis, S. Emission color tuning and phase transition determination based on high-pressure up-conversion luminescence in YVO_4 : Yb^{3+}, Er^{3+} nanoparticles. *J. Lumin.* **2019**, *209*, 321–327. https://doi.org/10.1016/j.jlumin.2019.02.008

Yang, L.; Peng, S.; Zhao, M.; Yu, L. New synthetic strategies for luminescent YVO_4 :Ln^{3+} (Ln = Pr, Sm, Eu, Tb, Dy, Ho, Er) with mesoporous cell-like nanostructure . *Opt. Mater. Express* **2018**, *8*, 3805–3819. https://doi.org/10.1364/OME.8.003805

Yu, M.; Lin, J.; Wang, Z.; Fu, J.; Wang, S.; Zhang, H. J.; Han, Y. C. Fabrication, patterning, and optical properties of nanocrystalline YVO_4 :A (A = Eu^{3+}, Dy^{3+}, Sm^{3+}, Er^{3+}) phosphor films via sol-gel soft lithography. *Chem. Mater.* **2002**, *14*, 2224–2231. https://doi.org/10.1021/cm011663y

Zhang, Y.-m.; Li, Y.-h; Li, P.; Hong, G.-y.; Yu, Y.n. Preparation and upconversion luminescence of YVO_4:Er_{3+}, Yb_{3+}. *Int. J. Miner. Metall. Mater.* **2010**, *17*, 225–228. https://doi.org/10.1007/s12613-010-0218-7